Supporting Information

Achieving the Selectivity of Oxygen Reduction Reactions by Regulating Electron Spin States and Active Centers on Fe-Mn-N_6-C Dual-atom Catalysts

Shiyao Li[1], Honghao Chen[4], Yue Qiu[5], Chengxing Cui[6,2], Wenhui Zhong[2,*], and Jun Jiang[3,*]

1. School of Chemistry and Chemical Engineering, Qufu Normal University, Qufu, Shandong 273165, P. R. China

2. Institute of intelligent innovation, Henan Academy of Sciences, Zhengzhou, Henan 451162, P. R. China

3. Key Laboratory of Precision and Intelligent Chemistry, School of Chemistry and Materials Science, University of Science and Technology of China, Hefei 230026, P. R. China

4. Department of Chemical Engineering, Tsinghua University, Beijing 100084, P. R. China

5. Grimwade Centre for Cultural Materials Conservation, School of Historical and Philosophical Studies, Faculty of Arts University of Melbourne Parkville, VIC 3052, Australia

6. School of Chemistry and Chemical Engineering, Institute of Computational Chemistry, Henan Institute of Science and Technology, Xinxiang, Henan 453003, P. R. China

The computations for SCPA spin population analysis

The formal name of SCPA is c^2 Population Analysis, which is a modified version of the Ros-Schuit equivalent Mulliken Population Analysis (MMPA) (*Theor. Chem. Acc.* 1966, 4, 1). In addition, SCPA spin distribution analysis was performed using the program Multiwfn 3.8 (*J. Comput. Chem.* **2012**, 33, 580), via the wave function file in Gaussian 16 package.

	$E_{(Fe-Mn)}$ (eV)	$E_{(N-C)}$ (eV)	$E_{(Fe-Mn@N-C)}$ (eV)	$E_{formation}$ (eV)
Fe-Mn-N_6-C(S=1/2)	**-6211.82**	**-65253.59**	**-71480.63**	**-15.23**
Fe-Mn-N_6-C(S=3/2)	**-6211.53**	**-65253.68**	**-71480.10**	**-14.88**
Fe-Mn-N_6-C(S=5/2)	**-6209.76**	**-65253.63**	**-71480.19**	**-16.80**
Fe-Mn-N_6-C(S=7/2)	**-6211.33**	**-65253.44**	**-71480.15**	**-15.38**
Fe-Mn-N_6-C(S=9/2)	**-6212.16**	**-65253.38**	**-71479.15**	**-13.69**

Table S1. The formation energy of Fe-Mn doped N-C in different spin states.

The formation energy for Fe-Mn incorporation (E_f) was obtained by the following equation:

$$E_f = E_{Fe-Mn@N-C} - E_{N-C} - E_{Fe-Mn}$$

where $E_{Fe-Mn@N-C}$ was the total energy of the Fe-Mn doped N-C, E_{N-C} was the energy of the N-C material substrate, and E_{Fe-Mn} was the total energy of the Fe-Mn dual atoms（*J. Am. Chem. Soc.* **2020**, 142, 12, 5709-5721）. Thus, the more negative the E_f value is, the greater the system's thermal stability. Therefore, the more negative E_f represents the greater the system's thermal stability. All energy adoptions are characterized by free energy.

Active Centers	Spin States	△E (eV)	△E(O_2) (eV)	△E(O_2+H) (eV)	△E(OOH) (eV)	△E(OOH-H) (eV)
Fe site	Fe-Mn-N_6-C(S=1/2)	0.00	0.07	0.00	0.00	0.09
	Fe-Mn-N_6-C(S=3/2)	0.53	0.27	0.22	0.01	0.37
	Fe-Mn-N_6-C(S=5/2)	0.44	0.18	0.06	0.04	0.00
	Fe-Mn-N_6-C(S=7/2)	0.49	0.00	0.01	0.13	0.08
	Fe-Mn-N_6-C(S=9/2)	1.40	0.07	0.02	0.26	0.14
Mn site	Fe-Mn-N_6-C(S=1/2)	0.00	0.00	0.41	0.00	0.00
	Fe-Mn-N_6-C(S=3/2)	0.53	0.54	0.03	0.13	0.62
	Fe-Mn-N_6-C(S=5/2)	0.44	0.33	0.00	0.13	0.31
	Fe-Mn-N_6-C(S=7/2)	0.49	0.36	0.17	0.54	0.56
	Fe-Mn-N_6-C(S=9/2)	1.40	0.69	1.21	1.11	1.10
Fe,Mn site	Fe-Mn-N_6-C(S=1/2)	0.00	0.00	0.18	0.00	0.00
	Fe-Mn-N_6-C(S=3/2)	0.53	0.28	0.00	0.08	0.55
	Fe-Mn-N_6-C(S=5/2)	0.44	0.25	0.02	0.06	0.00
	Fe-Mn-N_6-C(S=7/2)	0.49	0.22	0.64	0.39	0.28
	Fe-Mn-N_6-C(S=9/2)	1.40	0.54	0.44	0.52	0.96

Table S2. Energies of each system relative to its corresponding energy of spin ground state ($\Delta E=E_{system} - E_{ground}$).

Active Centers	Spin States	μ_B (catalyst)(μ_B)
Fe site	Fe-Mn-N_6-C(S=1/2)	-3.90
	Fe-Mn-N_6-C(S=3/2)	0.70
	Fe-Mn-N_6-C(S=5/2)	3.35
	Fe-Mn-N_6-C(S=7/2)	3.66
	Fe-Mn-N_6-C(S=9/2)	3.88
Mn site	Fe-Mn-N_6-C(S=1/2)	4.79
	Fe-Mn-N_6-C(S=3/2)	4.41
	Fe-Mn-N_6-C(S=5/2)	4.20
	Fe-Mn-N_6-C(S=7/2)	4.98
	Fe-Mn-N_6-C(S=9/2)	4.88
Fe,Mn site	Fe-Mn-N_6-C(S=1/2)	0.90
	Fe-Mn-N_6-C(S=3/2)	5.10
	Fe-Mn-N_6-C(S=5/2)	7.55
	Fe-Mn-N_6-C(S=7/2)	8.64
	Fe-Mn-N_6-C(S=9/2)	8.76

Table S3. The magnetic moments of Fe-Mn-N_6-C catalyst at different active sites and spin states.

Spin states	Activate site	O-O(Å)
S=1/2	Fe site	1.38
	Mn site	1.40
	Fe, Mn site	1.40
S=3/2	Fe site	1.38
	Mn site	1.39
	Fe, Mn site	1.41
S=5/2	Fe site	1.37
	Mn site	1.39
	Fe, Mn site	1.42
S=7/2	Fe site	1.31
	Mn site	1.38
	Fe, Mn site	1.38
S=9/2	Fe site	1.32
	Mn site	1.31
	Fe, Mn site	1.31

Table S4. The bond length of O-O bond under different spin states after structural optimization (the free O_2 molecular bond length is 1.21 Å).

Active Centers	Spin States	E_{des} (eV)
Fe site	Fe-Mn-N_6-C(S=1/2)	1.29
	Fe-Mn-N_6-C(S=3/2)	0.06
	Fe-Mn-N_6-C(S=5/2)	0.06
	Fe-Mn-N_6-C(S=7/2)	0.04
	Fe-Mn-N_6-C(S=9/2)	-0.29
Mn site	Fe-Mn-N_6-C(S=1/2)	0.53
	Fe-Mn-N_6-C(S=3/2)	0.16
	Fe-Mn-N_6-C(S=5/2)	0.02
	Fe-Mn-N_6-C(S=7/2)	0.07
	Fe-Mn-N_6-C(S=9/2)	0.24
Fe,Mn site	Fe-Mn-N_6-C(S=1/2)	0.07
	Fe-Mn-N_6-C(S=3/2)	0.04
	Fe-Mn-N_6-C(S=5/2)	0.07
	Fe-Mn-N_6-C(S=7/2)	-0.01
	Fe-Mn-N_6-C(S=9/2)	0.16

Table S5. The desorption energy of H_2O_2 produced via the ORR $2e^-$ pathway on Fe-Mn-N_6-C.

The adsorption energy (E_{ads}) for the adsorbate was obtained by the following equation:

$$E_{ads} = E_{total} - E_{catalyst} - E_{adsorbate}$$

where E_{total} was the total energy of the catalyst with adsorbate, $E_{catalyst}$ was the energy of the catalyst, and $E_{adsorbate}$ was the total energy of the adsorbate. Therefore, the more negative E_{ads} represents the stronger interaction between the adsorbate and the catalyst.

Active Centers	Spin States	$\triangle E_{barrier}$ ($^*OOH \rightarrow {}^*O + {}^*OH$) (eV)	$\triangle E_{barrier}$ ($^*OOH + {}^*H \rightarrow {}^*H_2O_2$) (eV)	$\triangle E_{barrier}$ (eV)
Fe site	Fe-Mn-N_6-C(S=1/2)	0.05	-0.04	0.09
	Fe-Mn-N_6-C(S=3/2)	0.20	0.09	0.11
	Fe-Mn-N_6-C(S=5/2)	0.33	0.04	0.29
	Fe-Mn-N_6-C(S=7/2)	0.62	0.02	0.60
	Fe-Mn-N_6-C(S=9/2)	0.57	0.20	0.37
Mn site	Fe-Mn-N_6-C(S=1/2)	0.62	0.36	0.26
	Fe-Mn-N_6-C(S=3/2)	0.45	-0.06	0.51
	Fe-Mn-N_6-C(S=5/2)	0.53	0.00	0.53
	Fe-Mn-N_6-C(S=7/2)	0.50	0.02	0.48
	Fe-Mn-N_6-C(S=9/2)	0.84	0.09	0.75
Fe,Mn site	Fe-Mn-N_6-C(S=1/2)	0.00	0.36	-0.36
	Fe-Mn-N_6-C(S=3/2)	0.12	0.06	0.06
	Fe-Mn-N_6-C(S=5/2)	0.21	0.08	0.13
	Fe-Mn-N_6-C(S=7/2)	0.40	0.03	0.37
	Fe-Mn-N_6-C(S=9/2)	0.45	0.12	0.33

Table S6. The energy barriers of $4e^-$ ORR and $2e^-$ ORR at different active sites and spin states on Fe-Mn-N_6-C, as well as the difference between the energy barriers of the two pathways.

The difference between the energy barriers of the $4e^-$ ORR and $2e^-$ ORR ($\triangle E_{barrier}$) was obtained by the following equation:

$$\triangle E_{barrier} = \triangle E_{barrier}(^*OOH \rightarrow {}^*O + {}^*OH) - \triangle E_{barrier}(^*OOH + {}^*H \rightarrow {}^*H_2O_2)$$

where $\triangle E_{barrier}(^*OOH \rightarrow {}^*O + {}^*OH)$ is the energy barrier of the key steps of 4e- ORR, $\triangle E_{barrier}(^*OOH + {}^*H \rightarrow {}^*H_2O_2)$ is the energy barrier of the key steps of $2e^-$ ORR.

Active Centers	Spin States	Δq (M+*OOH)(e-)	Δq (M+*OOH-H)(e-)	△$E_{barrier}$ (eV)
Fe site	Fe-Mn-N_6-C(S=1/2)	-0.57	-0.61	0.09
	Fe-Mn-N_6-C(S=3/2)	-0.29	-0.32	0.11
	Fe-Mn-N_6-C(S=5/2)	-0.49	-0.64	0.29
	Fe-Mn-N_6-C(S=7/2)	-0.18	-0.58	0.60
	Fe-Mn-N_6-C(S=9/2)	-0.21	-0.26	0.37
Mn site	Fe-Mn-N_6-C(S=1/2)	-0.61	-0.66	0.26
	Fe-Mn-N_6-C(S=3/2)	-0.42	-0.58	0.51
	Fe-Mn-N_6-C(S=5/2)	-0.44	-0.51	0.53
	Fe-Mn-N_6-C(S=7/2)	-0.59	-0.65	0.48
	Fe-Mn-N_6-C(S=9/2)	-0.62	-0.63	0.75
Fe,Mn site	Fe-Mn-N_6-C(S=1/2)	-0.77	-0.67	-0.36
	Fe-Mn-N_6-C(S=3/2)	-0.24	-0.41	0.06
	Fe-Mn-N_6-C(S=5/2)	-0.49	-0.50	0.13
	Fe-Mn-N_6-C(S=7/2)	-0.51	-0.80	0.37
	Fe-Mn-N_6-C(S=9/2)	-0.13	-0.67	0.33

Table S7. The electronic transfer before and after the adsorption of the active center M and *OOH(△q(M+*OOH)) in Fe-Mn-N_6-C-OOH, the electronic transfer before and after the adsorption of the active center M and *OOH intermediate in Fe-Mn-N_6-C-OOH-H ,as well as the difference between the energy barriers of 4e- ORR and 2e- ORR.

The difference between the energy barriers of the 4e- ORR and 2e- ORR ($\triangle E_{barrier}$) was obtained by the following equation:

$$\triangle E_{barrier} = \triangle E_{barrier}(^*OOH \rightarrow {}^*O + {}^*OH) - \triangle E_{barrier}(^*OOH + {}^*H \rightarrow {}^*H_2O_2)$$

where $\triangle E_{barrier}(^*OOH \rightarrow {}^*O + {}^*OH)$ is the energy barrier of the key steps of 4e- ORR, $\triangle E_{barrier}(^*OOH + {}^*H \rightarrow {}^*H_2O_2)$ is the energy barrier of the key steps of 2e- ORR.

Active Centers	Spin States	$\Delta\mu_B$ (M+*OOH)(μ_B)	$\Delta\mu_B$ (M+*OOH-H)(μ_B)	$\Delta\mu_B$ (μ_B)
Fe site	Fe-Mn-N_6-C(S=1/2)	0.83	1.20	-0.37
	Fe-Mn-N_6-C(S=3/2)	1.68	2.31	-0.63
	Fe-Mn-N_6-C(S=5/2)	0.14	1.07	-0.93
	Fe-Mn-N_6-C(S=7/2)	2.08	0.29	1.79
	Fe-Mn-N_6-C(S=9/2)	1.84	1.97	-0.13
Mn site	Fe-Mn-N_6-C(S=1/2)	0.54	0.59	-0.05
	Fe-Mn-N_6-C(S=3/2)	1.21	0.57	0.64
	Fe-Mn-N_6-C(S=5/2)	1.05	1.04	0.01
	Fe-Mn-N_6-C(S=7/2)	0.68	1.01	-0.33
	Fe-Mn-N_6-C(S=9/2)	0.64	0.45	0.19
Fe,Mn site	Fe-Mn-N_6-C(S=1/2)	0.77	0.67	0.10
	Fe-Mn-N_6-C(S=3/2)	0.24	0.41	-0.17
	Fe-Mn-N_6-C(S=5/2)	0.49	0.50	-0.10
	Fe-Mn-N_6-C(S=7/2)	0.51	0.80	0.29
	Fe-Mn-N_6-C(S=9/2)	0.13	0.67	0.54

Table S8. The variation of electron spin magnetic moments before and after the adsorption of the active center M and *OOH ($\Delta\mu_B$ (M+*OOH)) in Fe-Mn-N_6-C-OOH, the difference in electron spin magnetic moments before and after the adsorption of the active center M and *OOH ($\Delta\mu_B$ (M+*OOH)) in Fe-Mn-N_6-C-OOH-H, as well as the difference in electron spin magnetic moments before and after the adsorption of the *OOH intermediate on active site in both the $4e^-$ and $2e^-$ pathways which is denoted by $\Delta\mu_B = \Delta\mu_B$ (M+*OOH) - $\Delta\mu_B$ (M+*OOH-H).

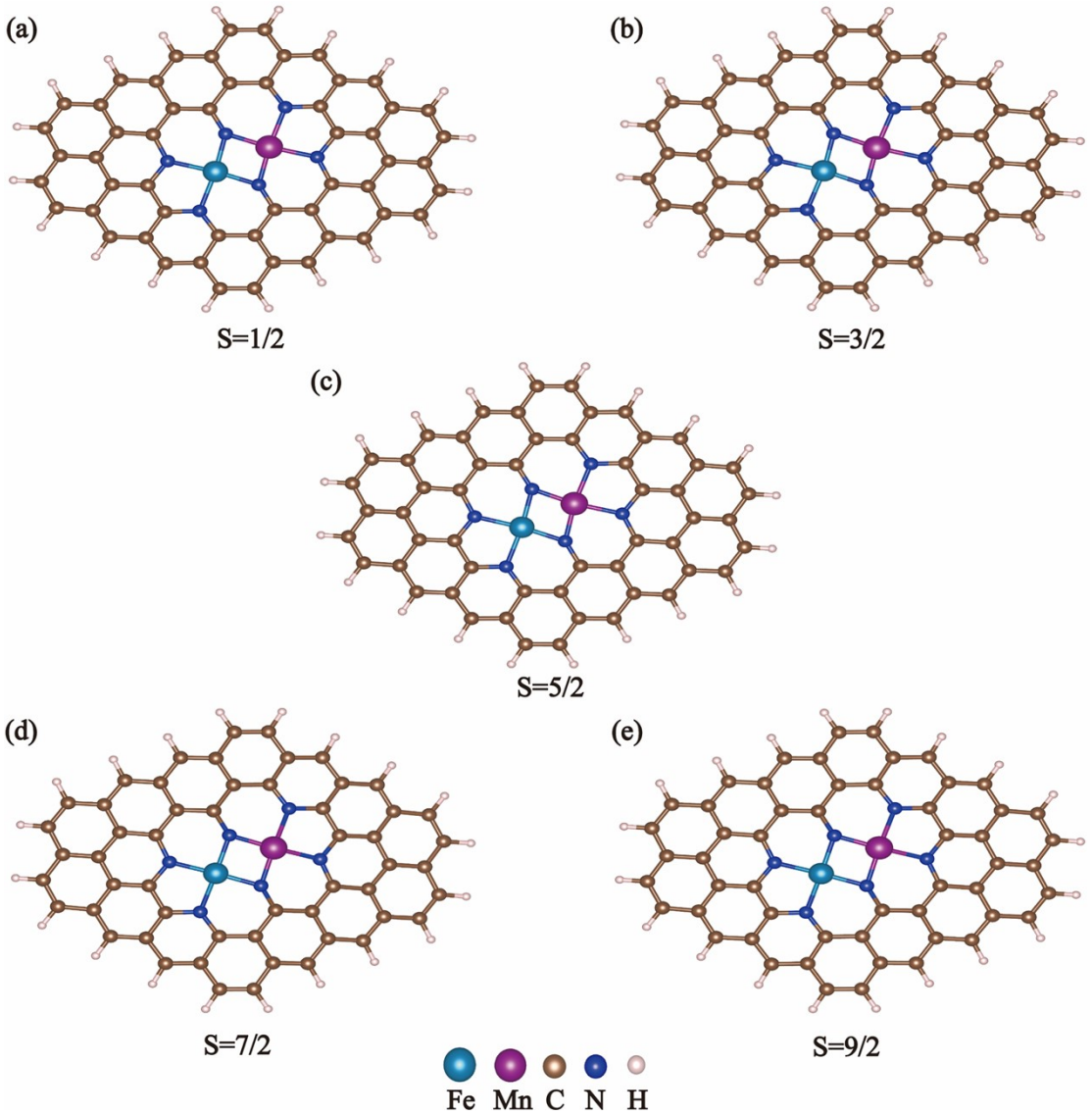

Fig. S1 Structures of Fe-Mn-N_6-C catalyst with different spin states (top view).

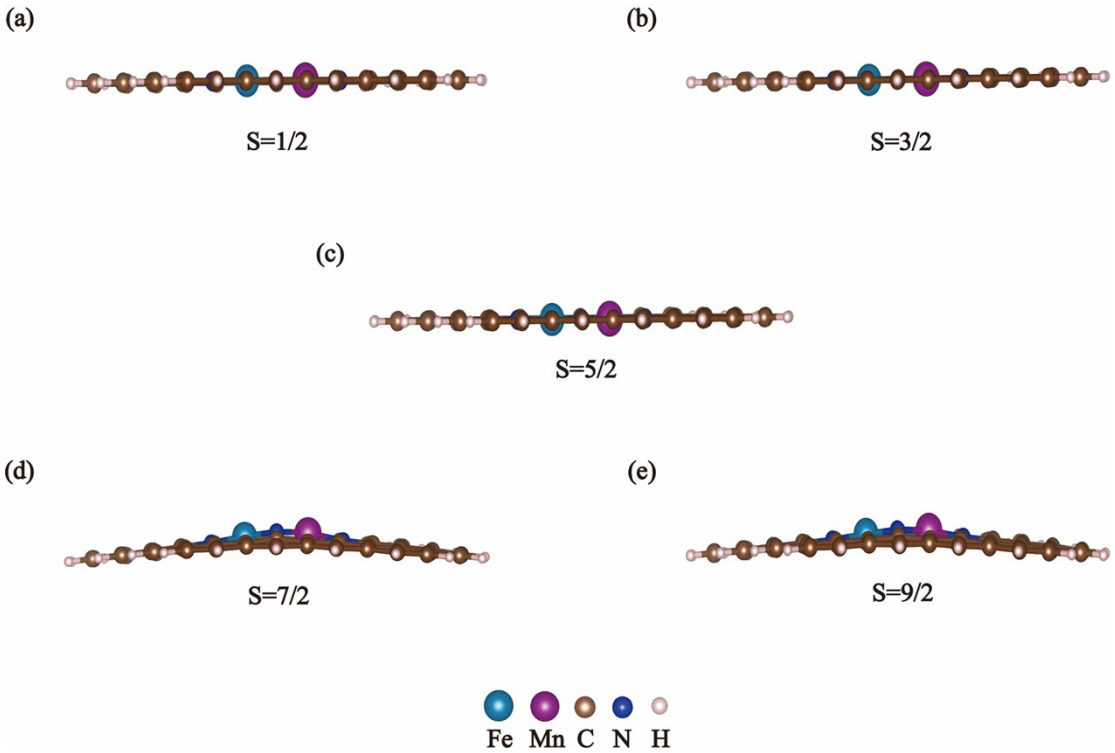

Fig. S2 Structures of Fe-Mn-N_6-C catalyst with different spin states (side view).

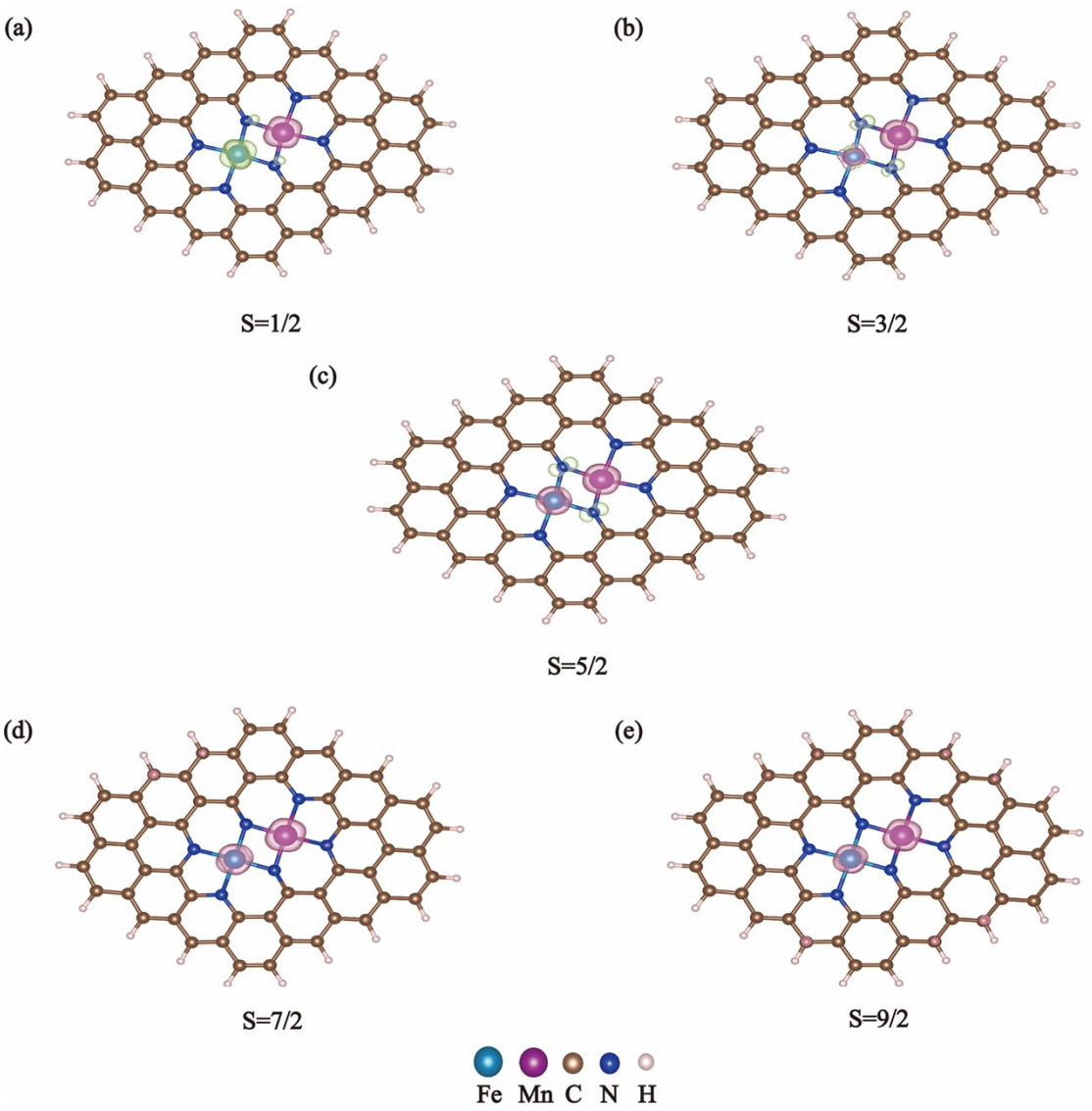

Fig. S3 Spin densities of Fe-Mn-N_6-C catalyst with different spin states. The isosurface value is 5×10^{-3} e Å^{-3}. Pink and green bubbles represent spin-up and spin-down, respectively.

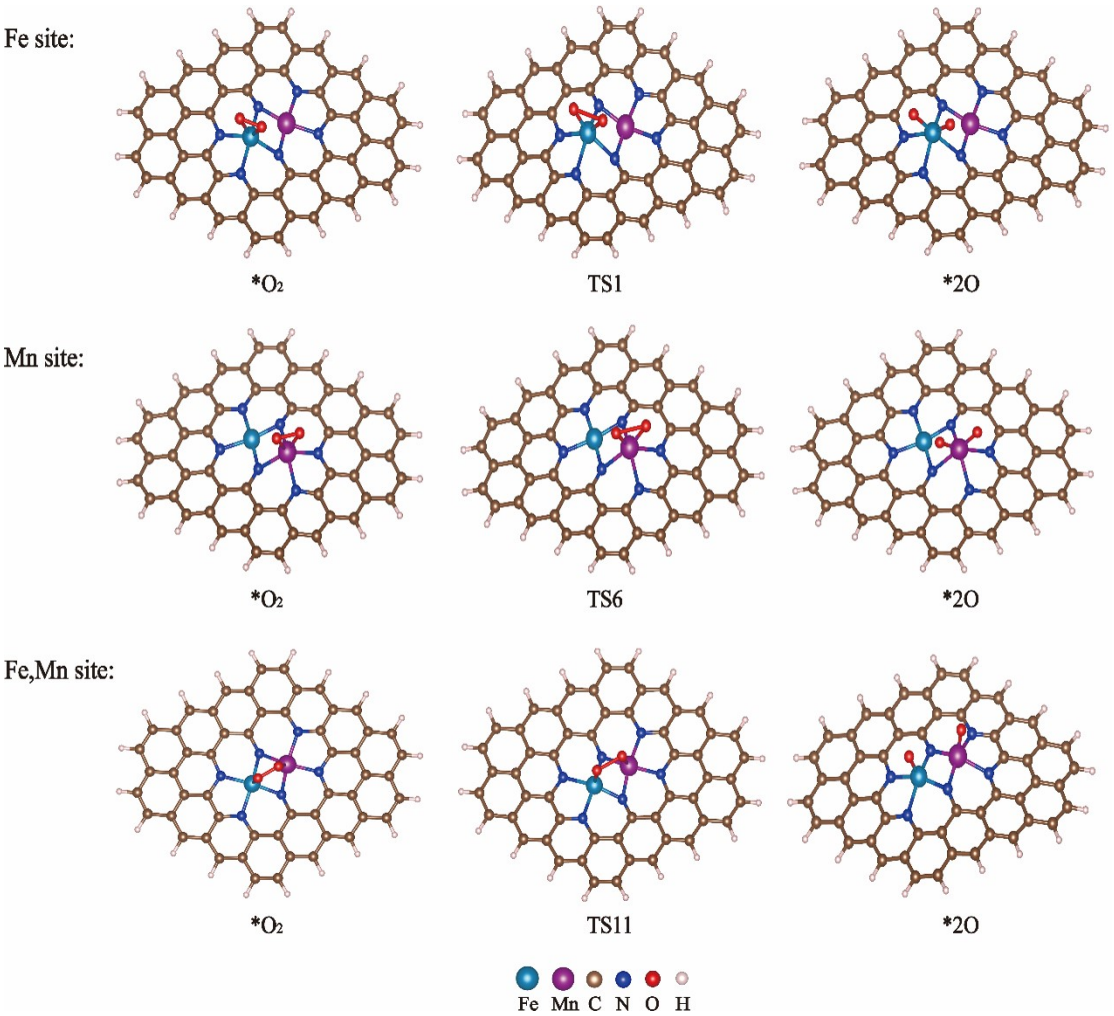

Fig. S4 Structures of intermediates and transition states involved in the optimal O_2 dissociation pathway on Fe-Mn-N_6-C.

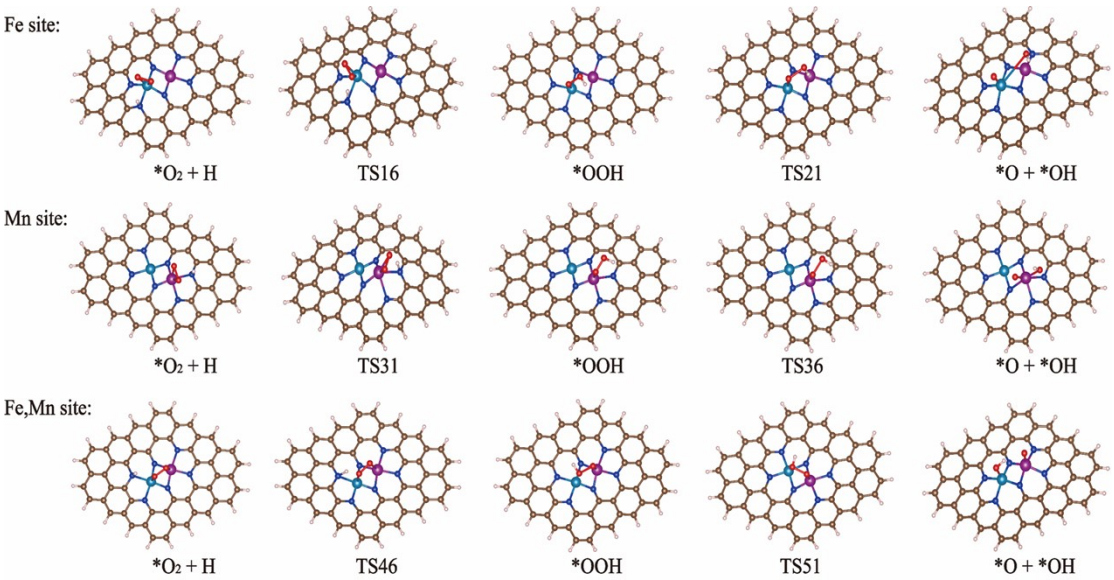

Fig. S5 Structures of intermediates and transition states involved in the optimal OOH pathway on Fe-Mn-N_6-C.

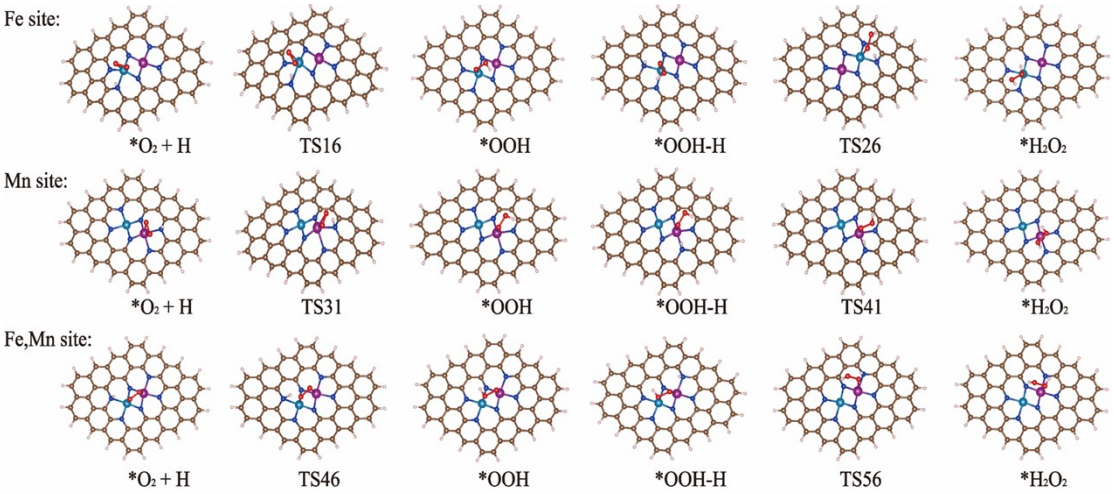

Fig. S6 Structures of intermediates and transition states involved in the optimal H_2O_2 pathway on Fe-Mn-N_6-C.

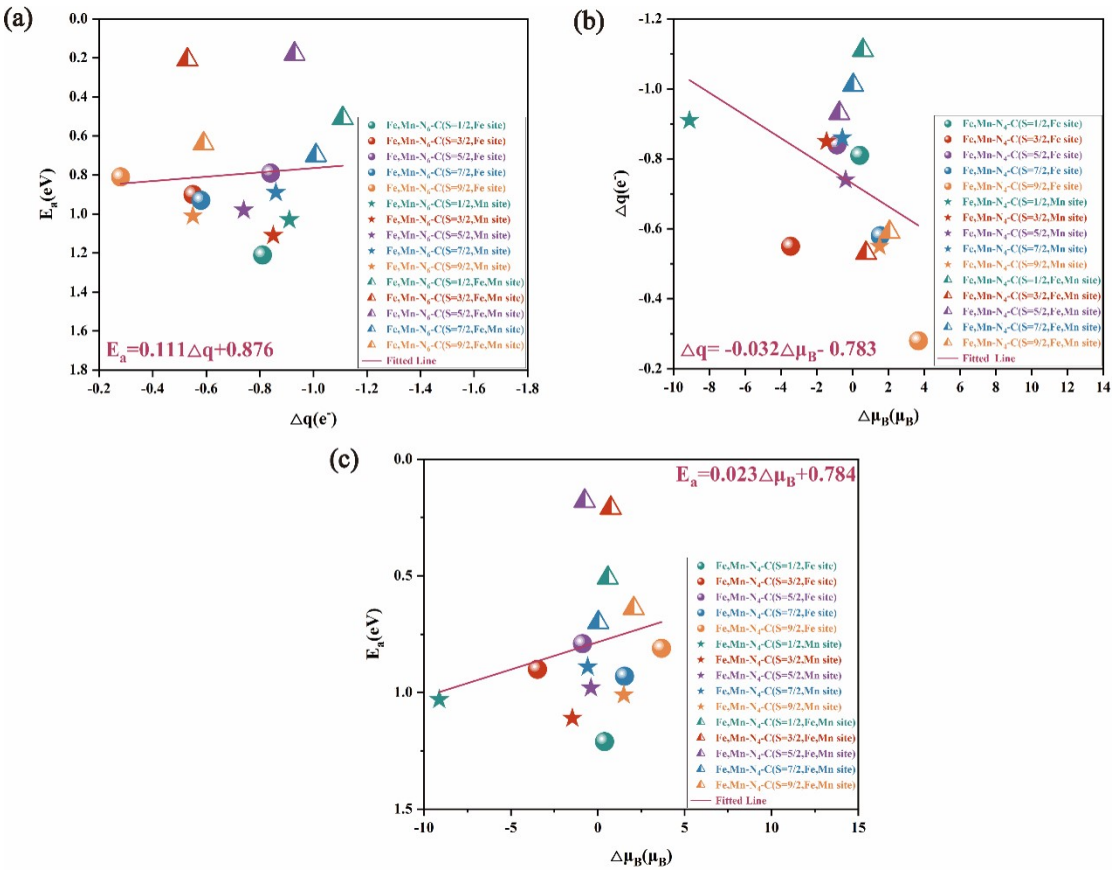

Fig. S7 Correlation between the charge difference of O_2 Δq and energy barriers of the rate-determining step of direct dissociation pathway of O_2 (a), coefficient of determination R^2 = 0.007; the change difference in electron spin magnetic moment △μ and electron transfer difference △q (b), coefficient of determination R^2 = 0.182; the change difference in electron spin magnetic moment △μ and energy barriers of the direct dissociation pathway of O_2 (c) , coefficient of determination R^2 = 0.052 , on Fe-Mn-N_6-C with different spin states.

We also analyzed the relationship between electron spin and electron transfer in different spin states of the Fe and Mn active centers of Fe-Mn-N_6-C, and O_2 molecules. The purpose is to explain why the presence of dual active sites significantly reduces the energy barrier of the direct O_2 dissociation pathway and facilitates the ORR reaction through the $4e^-$ pathway. This result suggests that rotation may not be the primary factor causing dissociation. The analysis presented in Figure S4 indicates that there is not a clear linear correlation between the electron spin magnetic moment and the energy barrier of the oxygen direct dissociation path rate control step. Additionally, the determination coefficient R^2 is observed to be very low.